Chapter 1

Photo-nuclear interactions

~~The~~ In ultra-peripheral heavy-ion collision, the colliding nuclei interact ~~electromagnetically in an ultra-peripheral heavy-ion collision~~only electromagnetically. In such events, no QGP state emerges, and the effects arising from the QGP no longer obscure the initial state effects. Other initial state probes such as peripheral nuclear collisions and proton-nucleus collisions have the potential to create the QGP obscuring which effects come from the initial state. ~~It is impossible to create the QGP in UPC events because the nucleons within the nucleus~~ In UPC events the nuclei do not collide, therefore final state effects coming from the QGP are not expected. Thus, UPC events provide clarity by enhancing physicists' understanding of the initial state.

In particular, these interactions between the field of photons surrounding the colliding nuclei and the gluons within the nuclei can produce a J/ψ, probing the gluon density. The J/ψ can be produced either coherently or incoherently. In the case of coherent interactions, the photon couples to the nucleus as a whole. In the incoherent case, the photon couples to the nucleons within the nucleus. The UPC J/ψ photoproduction cross section is therefore a probe of the initial state of the nucleus.

This cross section can be calculated using three steps. First, the Weizsäcker-Williams approximation provides a way to calculate the density of probing photons that surrounds the nucleus. Second, the electron-proton scattering data gives a value for the proton photoproduction cross sec-

tion at lower energies [?] . Last, a specific model is used to combined the previous two steps in order to calculate the nuclear photoproduction cross section. In this thesis the perterbutive Adeluyi and Bertulani (AB), STARlight, and the Leading Twist (LTA) models are discussed. Each of these methods handle the gluon density of the nucleus differently producing a measurable difference in the value of the J/ψ photoproduction cross section. Measurements at the LHC have provided important constrains to models of the nuclear gluon density. The analysis presented in Chapter **??** adds to the existing data in a new kinematic region. In this Chapter the theoretical framework for photon-nuclear interactions, together with an experimental review of recent results on ultra-peripheral heavy-ion collisions are described.

1.1 Weizsäcker-Williams approximation

The density of photons surrounding the colliding nuclei can be calculated using the Weizsäcker-Williams approximation. This approximation relates the electric field of a stationary point charge to the photon field that arises at ultra relativistic velocities. The approximation is semi-classical and combines both classical and quantum elements. In the Weizsäcker-Williams approximation, a Fourier transform of Maxwell's equations is combined with the quantum mechanical equation for the energy of the photon. The frequency modes of the electrostatic field are treated as photons. The

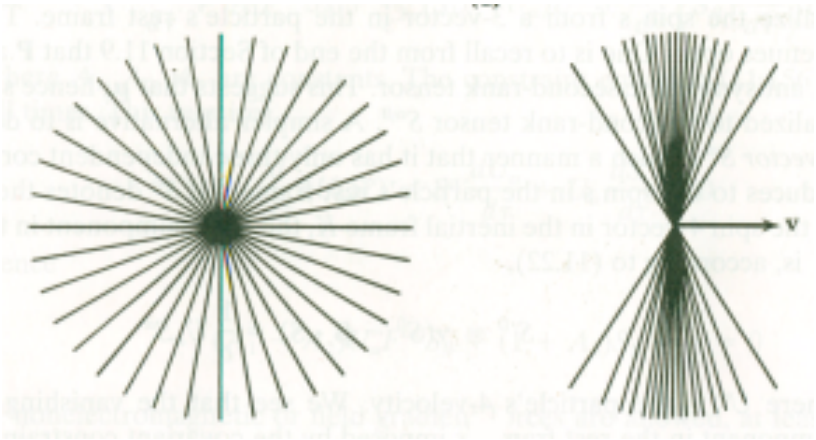

Figure 1.1: The electromagnetic field boosted and at rest.

Weizsäcker-Williams approximation makes the calculation of electromagnetic interactions with the nucleus tractable.

The Weizsäcker-Williams approximation begins with the equation for the electric field of the projectile nucleus at rest. To calculate the photon flux on the target nucleus, the electromagnetic field only needs to be considered at the position of the target nucleus. From the projectile's point of view, the target is moving and contributes $-vt$ to Eq. 1.1, the equation for the electric field of the projectile nucleus at rest.

$$x' = -vt', \qquad y' = b, \qquad z' = 0, \qquad \vec{\mathbf{E}}' = \left(\frac{eZ}{4\pi\varepsilon_0 \left((-vt')^2 + b^2 \right)^{3/2}} \right) \left(-vt'\hat{\mathbf{x}}' + b\hat{\mathbf{y}}' \right), \quad (1.1)$$

where b is the impact parameter defined as the distance of separation at closest approach, v is the velocity of the projectile nucleus, Z is the number of protons in the nucleus, and e is the charge of the electron. Two simplifications occur due to the choice of coordinates in Eq. 1.1. The magnetic field is equal to zero, as the projectile is at rest, and the z coordinate can be ignored, reducing the equation to two dimensions.

The Lorentz transformation converts the field equations in the projectile's frame to equations in the target's frame. Eq. 1.2 gives the result of the transformation from the projectile's primed frame to the target's rest frame for the field components [**?**]:

$$\begin{aligned} E'_x &= E_x, \qquad \gamma\left(E'_y/c + \beta B'_z\right) = E_y/c, \qquad \gamma\left(E'_z/c = \beta B'_y\right) = E_z/c, \\ B'_x &= B_x, \qquad \gamma\left(B'_y - \beta E'_z/c\right) = B_y, \text{ and} \qquad \gamma\left(B'_z + \beta E'_y/c\right) = B_z. \end{aligned} \quad (1.2)$$

The transformation equations for the fields, Eq. 1.2, and the transformation of the coordinates reduce to Eq. 1.3 [**?**]:

$$\begin{aligned} E'_x = E_x, \qquad \gamma E'_y = E_y, \qquad \gamma\beta E'_y/c = B_z, \\ ct' = \gamma ct, \text{ and} \qquad x' = -\gamma\beta ct. \end{aligned} \quad (1.3)$$

The Lorentz transformation reduces the six components of the electromagnetic field in the target's frame to the three equations in Eq. 1.2 by relating them to the fields ~~of~~ in the projectile's frame.

By combining Eq. 1.1 and Eq. 1.2, equations for the electric and magnetic fields in the target's rest frame are obtained

$$\vec{\mathbf{E}} = \left(\frac{\gamma e Z}{4\pi\varepsilon_0 \left((\gamma v t)^2 + b^2 \right)^{3/2}} \right) (vt\hat{\mathbf{x}} + b\hat{\mathbf{y}}), \text{ and}$$
$$\vec{\mathbf{B}} = \frac{\gamma\beta e Z b}{4\pi c\varepsilon_0 \left((\gamma v t)^2 + b^2 \right)^{3/2}} \hat{\mathbf{z}} = \frac{\gamma\mu_0 v e Z b}{4\pi \left((\gamma v t)^2 + b^2 \right)^{3/2}} \hat{\mathbf{z}}. \tag{1.4}$$

If the impact parameter b goes to zero, the target sits in the line of the projectile particle's motion, and the denominator carries a factor of γ squared. When vt goes to zero, the projectile particle position lays on the y-axis, and the numerator carries a factor of γ. This results in fields that are a factor of γ^3 higher in the y direction than in the x direction (see Fig. 1.1). The boost compresses the electric field of the charge in the direction of the boost and produces a magnetic field resulting in a form similar to radiation. The point charge at ultra relativistic velocities produces a strong electric field in the plane transverse to its motion resembling a plane wave.

Separating the electromagnetic field into even and odd functions of time ~~simplify~~ simplifies the decomposition of the field equations into Fourier frequency modes. The even functions decompose into cosine functions, odd functions into sine functions. The y-component of the electric field and the z-component of the magnetic field are even functions in time, and the x-component of the electric field is an odd function in time. Eq. 1.5 gives the Fourier transformation integrals.

$$E_x(\omega) = \sqrt{\frac{2}{\pi}} \frac{eZ}{4\pi\varepsilon_0 b^2} \int_0^\infty \frac{(\gamma v t/b)\sin(\omega t)}{\left((\gamma v t/b)^2 + 1 \right)^{3/2}} dt,$$
$$E_y(\omega) = \sqrt{\frac{2}{\pi}} \frac{\gamma eZ}{4\pi\varepsilon_0 b^2} \int_0^\infty \frac{\cos(\omega t)}{\left((\gamma v t/b)^2 + 1 \right)^{3/2}} dt, \text{ and} \tag{1.5}$$
$$B_z(\omega) = \frac{\beta E_y(\omega)}{c}.$$

The solutions to the integrals of Eq. 1.5 are the following [**?**]:

$$u = \frac{\gamma v t}{b}, \qquad du\left(\frac{b}{\gamma v}\right) = dt, \qquad \omega' = \frac{\omega b}{\gamma v},$$
$$\int_0^\infty \frac{u\sin(\omega' u)}{(u^2+1)^{3/2}} du = \omega' K_0(\omega'), \text{ and} \qquad \int_0^\infty \frac{\cos(\omega' u)}{(u^2+1)^{3/2}} = \omega' K_1(\omega'). \tag{1.6}$$

In Eq. 1.6, ω can be related to the energy of a photon by $E = \hbar\omega$. The components of the electric field in terms of ω are:

$$E_x(\omega) = \sqrt{\frac{2}{\pi}} \frac{eZ}{4\pi\varepsilon_0 b^2} \frac{b}{\gamma v} \frac{\omega b}{\gamma v} K_0\left(\frac{\omega b}{\gamma v}\right), \text{ and} \qquad E_y(\omega) = \sqrt{\frac{2}{\pi}} \frac{\gamma eZ}{4\pi\varepsilon_0 b^2} \frac{b}{\gamma v} \frac{\omega b}{\gamma v} K_1\left(\frac{\omega b}{\gamma v}\right). \tag{1.7}$$

The y-component of the electric field does not have a factor of t in the numerator in Eq. 1.5, therefore the factor of γ remains outside of the integral ~~.~~ for the Bessel functions in Eq. 1.7. In Eq. 1.7, E_y carries an additional factor of γ in the numerator relative to the E_x, therefore in the case when $\gamma >> 1$, E_x can be neglected.

When v approaches c, $\beta \approx 1$, the y-component of the electric field and the z-component of the magnetic field are related by a factor of c, $E_y/c = B_z$. E_y is approximately equally to γE_x because $K_0(x)$ is smaller than $K_1(x)$ for all x. The conditions imposed by the ultra-relativistic limit result in the following relationship

$$\gamma \gg 1 \Rightarrow \gamma E_x \gg E_x \Rightarrow E_y \gg E_x. \tag{1.8}$$

The six field components are reduced to one electric component and one perpendicular magnetic field component, which have a configuration identical to a plane wave.

As with plane waves, the energy per area per time transferred by the electromagnetic field is given by the Poynting vector. The Poynting vector takes the simple form of a plane pulse propagating in the x direction as given by

$$\vec{\mathbf{S}} \equiv \vec{\mathbf{E}} \times \vec{\mathbf{B}}/\mu_0 = \left(E_y^2/c\mu_0\right)\hat{\mathbf{x}} = c\varepsilon_0 E_y^2 \hat{\mathbf{x}}. \tag{1.9}$$

The Poynting vector relates to the fluence (energy per unit area) by the expression [**?**]

$$I(b) = \hat{\mathbf{x}} \cdot \int_0^\infty \vec{\mathbf{S}} d\omega = \int_0^\infty \left(c\varepsilon_0 E_y^2\right) d\omega = \int_0^\infty \left(\frac{dI}{d\omega}\right) d\omega, \tag{1.10}$$

and the spectral fluence (energy per area per frequency) is given by

$$\frac{dI}{d\omega} = c\varepsilon_0 E_y^2 = \frac{e^2 Z^2 c}{4\pi^3 b^2 v^2 \varepsilon_0} \left(\frac{\omega b}{\gamma v}\right)^2 K_1^2\left(\frac{\omega b}{\gamma v}\right) = \alpha\hbar \left(\frac{Z}{b\beta\pi}\right)^2 \left(\frac{\omega b}{\gamma v}\right)^2 K_1^2\left(\frac{\omega b}{\gamma v}\right). \tag{1.11}$$

The spectral fluence given by Eq. 1.11 relates the frequency to energy. The quantum mechanical equation, $E = \hbar\omega$, gives the energy of a photon, which is related to the spectral fluence. The relationship between the photon number density and the spectral fluence is [**?**]

$$\frac{dI}{d\omega} d\omega = \hbar\omega N(\omega) d(\hbar\omega) \Rightarrow \frac{1}{\hbar^2\omega} \frac{dI}{d\omega} = N(\omega). \tag{1.12}$$

Substituting Eq. 1.11 into Eq. 1.12 yields the semiclassical photon flux:

$$N(\omega, b) = \frac{\alpha}{\hbar\omega} \left(\frac{Z}{b\beta\pi}\right)^2 \left(\frac{\omega b}{\gamma v}\right)^2 K_1^2\left(\frac{\omega b}{\gamma v}\right). \tag{1.13}$$

This replaces the classical electric field of a point charge with a semiclassical field of photons. The photon flux in Eq. 1.13 provides the electromagnetic input to the J/ψ photoproduction cross section calculation.

1.2 The STARlight model

The STARlight model for calculating the J/ψ photoproduction cross section has three main components. The STARlight approach is constructed from the Weizsäcker-Williams photon flux, uses the vector meson dominance fit to the proton-electron data, and uses the Glauber model for calculating the nuclear cross sections from the proton-electron cross sections. The Weizsäcker-Williams photon flux provides the probe. The proton-electron scattering data combine with the Glauber model

create a picture of the initial state of the nucleus. Each of the different approaches discussed in this thesis to calculating the UPC J/ψ photoproduction cross section use these same elements. However, the different models each use the last two elements differently to produce different pictures of the nucleus and different cross sections values.

The photon flux in the photoproduction cross section calculation must be finite in order for the cross section to be meaningful. The Weizsäcker-Williams approximation, Eq. 1.13, diverges at $b = 0$. The probability of the nuclei interacting would exceed one if the photon flux were infinite. Special treatment of impact parameter, b, where the colliding nuclei overlap eliminates the divergency.

A convolution of the photon flux with the nucleon number density functions removes the divergency at $b = 0$. The nucleon density of a single nucleus is given by

$$\rho_A(s) = \frac{\rho_0}{1 + exp[(s - R_{WS})/d)]}, \tag{1.14}$$

where s is the distance from the center of the nucleus, R_{WS} is the radius of the nucleus, and d is the skin depth, which determines how quickly the nucleon density falls off beyond the nuclear radius. In Eq. 1.15 the depth of the nucleus is integrated out leaving just the transverse dimension in T_A. The average number of nucleons in the overlap region is given by a convolution of T_A from each of the two nuclei to produce The average number of nucleons in the overlap region is given by a convolution of T_A from each of the two nuclei to produce nuclear overlap integral, T_{AA},

$$\begin{aligned} T_A(\vec{r}) &= \int dz \rho_A(\sqrt{|\vec{r}|^2 + z^2}), \text{ and} \\ T_{AA}(|\vec{b}|) &= \int d^2\vec{r} T_A(\vec{r}) T_A(\vec{r} - \vec{b}). \end{aligned} \tag{1.15}$$

For a given impact parameter b, the product of $T_{AA}(|\vec{b}|)$ and σ_{NN} gives the average number of nucleon-nucleon collisions. It is T_{AA} that modulates the photon flux. As input to the Poisson distribution, T_{AA} reduces Eq. 1.13 at values of b where the nuclei overlap significantly and eliminates the divergency in the photon flux.

The convolution of the photon flux with the b-dependent probability that no nucleon-nucleon collisions occur removes the divergency in Eq. 1.13.

The Poisson distribution gives the probability that no collisions occur at a given b using the mean number of nucleons in the overlap region given by T_{AA}:

$$P_0(b) = exp[-T_{AA}(b)\sigma_{NN}], \tag{1.16}$$

where σ_{NN} is the cross section for a nucleon-nucleon interaction, which gives the probability that a collision will occur given the average number of nucleons in the overlap region. The ~~average photon flux~~ photon flux is averaged over impact parameter ~~can be calculated from the~~ by integration of the b-dependent photon flux ~~with~~ multiplied by the b-dependent probability of having no nucleon-nucleon interactions:

$$\frac{dN_\gamma(k)}{dk} = \int_0^\infty 2\pi b db P_0(b) \int_0^R \frac{rdr}{\pi R_A^2} \int_0^{2\pi} d\phi \frac{d^3N_\gamma(k, b + r\cos(\phi))}{dk d^2r}. \tag{1.17}$$

Although Eq. 1.17 goes down to $b = 0$ where the photon flux is infinite, the fact that the probability of having a nucleon-nucleon collisions is high eliminates the divergency.

A power-law fit to the proton photoproduction data gives an analytic expression for the energy dependence of the proton photoproduction cross section. The fitting function depends on the photon-proton center of mass energy. The parameterization of the forward proton photoproduction cross section fit:

$$\left.\frac{d\sigma(\gamma p \to Vp)}{dt}\right|_{t=0} = b_v(XW^\varepsilon + YW^{-\eta}), \tag{1.18}$$

where W is the center of mass energy of the proton-photon system in Eq. 1.18. The remaining variables in Eq. 1.18 are power-law fit parameters. The XW^ε term characterizes pomeron mediated interactions, and the YW^η term characterizes meson mediated interactions [**?**]. J/ψ's high mass relative to the π and ρ^0 renders the second term in Eq. 1.18 negligible as the term falls rapidly with increasing W. Eq. 1.18 allows for extrapolation and interpolation of the measured forward

proton photoproduction cross section. The fit to the data provides estimates for energies that have not yet been probed experimentally. The proton photoproduction cross sections from the electron-proton scattering data is a direct input to the STARlight model. In this method, a power-law fit to the proton photoproduction data is the input for the Glauber calculation.

Vector meson dominance and the optical theorem allow for the calculation of the total proton-meson scattering cross section from the fit given by Eq. 1.18. The optical theorem relates the total cross section, σ, to the corresponding forward scattering cross section, $d\sigma/dt|_{t=0}$, where t is the momentum transfer squared. The most likely fluctuations of the photon are to vector mesons because of the quantum numbers of the photon. Due to this consideration, vector meson dominance asserts that only the vector meson fluctuations of the photon need to be considered. The forward scattering cross section is given by the following

$$\frac{d\sigma(\gamma p \to Vp)}{dt}\Big|_{t=0} = \frac{4\pi\alpha}{f_v^2(M_V,\Gamma_{l^+l^-})}\frac{d\sigma(Vp \to Vp)}{dt}\Big|_{t=0},$$
$$\sigma(Vp)^2_{tot} = 16\pi\frac{d\sigma(Vp \to Vp)}{dt}\Big|_{t=0}, \tag{1.19}$$

where M_V, is the mass of the vector meson, and $\Gamma_{l^+l^-}$, is leptonic decay width. The result of combining vector meson dominance and the optical theorem in Eq.1.19 provides the cross section for a meson to scatter off a proton.

The Glauber model allows for Eq. 1.19, the proton-meson scattering cross section, to be used to calculate a nucleus-meson scattering cross section. The Glauber model is used to calculate nuclear cross sections from nucleon interaction cross sections by use of T_{AA}. The combination of the mean number of nucleons in the overlapping region of a nucleus-nucleus collision, T_{AA}, the nucleon cross section, σ, and the Poisson distribution make-up the core of the Glauber model. For the total nucleus-meson scattering cross section, the equation has the following form:

$$\sigma_{tot}(VA) = \int d^2\vec{r}(1 - e^{-\sigma_{tot}(Vp)T_{AA}(\vec{r})}). \tag{1.20}$$

In Eq. 1.20, the term $e^{\sigma_{tot}(Vp)T_{AA}}$ gives the probability of having no meson-nucleon scatterings from the Poisson distribution. The probability of having at least one scattering is given by subtracting one from the term $e^{\sigma_{tot}(Vp)T_{AA}}$ in Eq. 1.20.

Reversing the process used for the proton, Eq. 1.20, the meson nucleus scattering cross section, relates to forward nuclear photoproduction cross section through the optical theorem. Using the optical theorem, the nuclear photoproduction cross section is given by

$$\begin{aligned} \frac{d\sigma(\gamma A \to VA)}{dt}\Big|_{t=0} &= \frac{\alpha\sigma_{tot}^2(VA)}{4\pi f_v^2}, \\ \sigma(\gamma A \to VA) = \frac{d\sigma(\gamma A \to VA)}{dt}\Big|_{t=0} &\int_{t_{min}}^{\infty} dt|F(t)|^2, \end{aligned} \tag{1.21}$$

where F is the Fourier transform of the nuclear density function, ρ_A. Eq. 1.21 is joined with the photon flux incident on the nucleus resulting in the following

$$\sigma(AA \to AAV) = 2\int dk \frac{dN_\gamma}{dk}\sigma(\gamma A \to VA). \tag{1.22}$$

The factor of 2 in Eq. 1.22 comes from the fact that both of the two colliding nuclei contribute. Vector meson production rates in UPC collisions can be calculated by Eq. 1.22. In this thesis the measured UPC J/ψ cross section is compared to the STARlight predictions.

1.3 The Adeluyi and Bertulani model

To calculate the UPC J/ψ photoproduction cross section, the Adeluyi and Bertulani model uses the nuclear gluon density to characterize the nucleus and the Weizsäcker-Williams approximation for the probing photon flux. The AB method combines these components such that the nuclear gluon density is a direct variable. The nuclear gluon density term in the AB formulation allows for the use of a variety of nuclear gluon density models. A range of nuclear gluon densities are present in the available models resulting in a wide range of possible cross section values. The UPC J/ψ photoproduction cross section is correlated with the gluon density of the nucleus, increasing with

higher densities and decreasing with lower densities. In the AB approach, the calculation of the UPC J/ψ photoproduction cross section allows experiments to constrain many different nuclear gluon density models.

In the AB method, the photon interacts with the nucleus by fluctuating to a quark-anitquark pair. For J/ψ, the photon fluctuates to a $c\bar{c}$ pair. The probability for the photon to fluctuate to a $c\bar{c}$ pair depends on the $M_{J/\psi}$, the mass of J/ψ, $\Gamma_{l^+l^-}$, the J/ψ leptonic decay width, and α, the electromagnetic coupling constant. These three variables connect the c quark to the electromagnetic force mediator, the photon. Recast as a $c\bar{c}$ pair, the photon couples to the nuclear gluon density. The AB method uses the fluctuation of the photon to a $c\bar{c}$ pair as the foundation for calculating the forward J/ψ photoproduction cross section.

The $c\bar{c}$ pair arising from the photon fluctuation scatters off the gluons of the nucleus. The density of gluons in the nucleus determines how likely and therefore how large the cross section is for the quarks to scatter and form a J/ψ. The forward scattering cross section is the portion of those scattering events which transfer the minimum amount of momentum between the photon and the nucleus. The forward cross section for J/ψ photoproduction in the nucleus has the following form [**?**]:

$$\left.\frac{d\sigma_{\gamma A\to J/\psi A}}{dt}\right|_{t=0} = \xi_{J/\psi}\left(\frac{16\pi^3\alpha_s^2\Gamma_{l^+l^-}}{3\alpha M_{J/\psi}^5}\right)[xG_A(x,\mu^2)]^2, \tag{1.23}$$

where $\xi_{J/\psi}$ is an experimentally derived correction factor, α_s is the strong coupling constant, x is the momentum faction of the nucleus the scattering gluons carry, and G_A is the gluon density of the nucleus. Both the c and $\bar{c}$ couple to the gluon density, and the double coupling results in the squared dependence of the cross section on the gluon density in Eq. 1.23. Fitting Eq. 1.23 to proton-electron scattering data sets $\xi_{J/\psi}$ [**?**]. The forward scattering cross section given by Eq. 1.23 connects the photon flux to the gluon density and provides the input to calculate the total cross section by the optical theorem.

The optical theorem relates the forward cross section in Eq. 1.23 to the total photoproduction cross section. The total cross section gives the probability that a photon incident on the nucleus will produce a J/ψ regardless of the momentum transfered in the interaction. The total cross section

equation is given by

$$\sigma_{\gamma A\to J/\psi A}(k) = \frac{d\sigma_{\gamma A\to J/\psi A}}{dt}\Big|_{t=0}\int_{t_{min}(k)}^{\infty} dt|F(t)|^2, \tag{1.24}$$

where $t_{min} = (M_{J/\psi}^2/4k\gamma_L)^2$, which is the minimum amount of momentum transfer required to produce a J/ψ given the photon wave number k. The k dependence of t_{min} translates to the rapidity dependence of the total cross section. The total cross section for photoproduction, Eq. 1.24, provides the input to Eq. 1.28, which gives the rapidity dependence of the UPC photoproduction cross section. Eq. 1.24 as input to Eq. 1.28 allows for experimental comparison of the AB method to measurements of UPC photoproduction cross sections. With the AB method's direct use of the nuclear gluon density in Eq. 1.23, the AB method allows for experimental exploration of any gluon density model.

1.4 Leading Twist Approach Derivation

The Leading Twist Approach is another method for calculating UPC photoproduction cross sections. Contrary to the STARlight model, the LTA model introduces additional nuclear effects originating from modification of the nuclear gluon density. The LTA method uses the Weizsäcker-Williams approximation to calculate the photon flux created by the colliding nuclei. As in the STARlight method, the probability of having no hadronic collisions modulates the flux. The photon flux for the LTA method has the following form [**?**]:

$$n_{\gamma/A}^i(\omega_\gamma) = \frac{2\alpha Z^2}{\pi}\int_{b_{min}}^{\infty} db\frac{x^2}{b}\Big[K_1^2(x) + \frac{K_0^2(x)}{\gamma_L^2}\Big]P_0(b)P_C^i(b), \tag{1.25}$$

where $x = \frac{\omega b}{\gamma_L}$, and $K_0^2(x)$ term contributes a photon flux in the transverse direction, and $P_C^i(b)$ is an modulation factor that requires various additional interactions. These interactions result in emission of neutrons from the receding nuclei as the nuclei relax from excited states. The terms P_C^i and K_0 provide additional ways to distinguish UPC events from nuclear collisions experimentally

but leave the underlying interaction mechanism the same. For example, the additional terms in the LTA formulation of the photon flux produce calculations of asymmetric neutron emission, which separate UPC events from nuclear collisions.

The LTA model derives the nucleon cross section from derivations of the nucleon gluon densities from electron-proton scattering data and leading order perturbative quantum field theory calculations. The forward photoproduction cross section of the nucleon has the following form [**?**]:

$$\frac{d\sigma_{\gamma N\to J/\psi N}(t=0)}{dt} = \frac{16\Gamma_{l^+l^-}\pi^3}{3\alpha M_{J/\psi}^5}[\alpha_s\mu^2 x G_N(x,\mu^2)]^2, \tag{1.26}$$

where G_N is the gluon density of the nucleon, x is the fraction of the nucleon's momentum the gluon carries, and μ is related to momentum at which the nucleon is being probed, which is equal to $M_{J/\psi}/2$ for J/ψ photoproduction. By connecting the gluon density to the cross section, Eq. 1.26 allows for the gluon density to be experimentally probed.

The LTA model exploits the optical theorem to relate the forward photoproduction cross section of the nucleon to the nuclear cross section. The relation is

$$\sigma_{\gamma A\to J/\psi A}(\omega) = \frac{d\sigma_{\gamma N\to J/\psi N}}{dt}(\omega,t_{min})R_g^2\int_{t_{min}}^{\infty}dt|F(t)|^2, \tag{1.27}$$

where R_g is the nuclear modification function, the ratio between the gluon density of the nucleon, G_N, to the gluon density of the nucleus, G_A. As with the STARlight method, the optical theorem relates the forward cross section, $\frac{d\sigma_{\gamma N\to J/\psi N}}{dt}(\omega,t_{min})$, to the total cross section, $\sigma_{\gamma A\to J/\psi A}$.

From Eq. 1.27, the LTA method can predict the angular distribution of photoproduced J/ψ with respect to the beam axis. The angular distribution is expressed in the form of the rapidity dependency of the UPC photoproduction cross section given by

$$\frac{d\sigma_{A_1A_2\to A_1A_2J/\psi}}{dy} = n_{\gamma/A_1}(y)\sigma_{\gamma A_2\to J/\psi A_2}(y) + n_{\gamma/A_2}(-y)\sigma_{\gamma A_1\to J/\psi A_1}(-y), \tag{1.28}$$

where $y = ln\left(\frac{2\omega}{M_{J/\psi}}\right)$. Eq. 1.28 is comprised of two terms, one for photons from the forward going

nucleus interacting with the backward going nucleus, and a second for the reverse situation. The integration of Eq. 1.28 over y produces the factor of 2 that is present in Eq. 1.22. The rapidity distribution of the photoproduction cross section given in Eq. 1.28 provides a more detailed prediction and allows for more direct experimental ~~comparison~~comparisons.

1.5 Photon-induced nuclear break-up

In addition to the photoproduction of quark anti-quark resonances such as the J/ψ, photo-nuclear interactions can also result in emission of a neutron from the struck target nucleus. To calculate the cross section for neutron emission in UPC events, the photon flux calculated from the Weizsäcker-Williams approximation is combined with the nuclear photon absorption cross section. The absorption of photons can be described by two processes, namely the Giant Dipole Resonance (GDR), and the dissociation of deuterium. In this section, the theoretical description of photon-induced nuclear break-up is discussed.

Following the formulation in [**?**], the cross section for a nucleus to absorb a photon, σ_{PN}, is given by

$$\sigma_{PN} = \sigma_{GDR} + \sigma_{QD}. \tag{1.29}$$

The Giant Dipole Resonance (GDR) cross section, σ_{GDR} is the result of the collective motion of the protons relative to the neutrons and dominates at lower photon frequencies. The Quasi-Deuterium (QD) cross section, σ_{QD}, represents the nucleus as a collection of proton-neutron pairs (deuterium) and dominates at higher photon energies.

There are two models for the GDR: the Goldhaber and Teller model, and the Steinwedel and Jensen model. Goldhaber and Teller treats the protons and neutrons as two separate and ridged density profiles that, when excited, oscillate with respect to each other [**?**]. Steinwedel and Jensen modeled the protons and neutrons as fluids contained in a single sphere that have shifting density profiles [**?**].

In the Goldhaber and Teller model, the potential that holds protons and neutrons together de-

pends on the difference of the neutron and proton densities squared. Assuming the neutron and proton densities have the same shape, if the two fully overlap, there is no difference in the densities and the potential energy is zero. If the two density distributions are separated, the overlap in the shape will not cancel. In the separated configuration, there will be a non-zero potential energy. The potential energy has the form of a harmonic oscillator with a spring constant that depends on the initial density distribution [**?**] given by

$$U = \frac{1}{2}Kz^2, \qquad K = k\int d^3r\,(\nabla\rho_0)^2\,. \tag{1.30}$$

If the nucleus has a shape cut off in density at its edge, then the integral is dominated by the region at the surface, and the spring constant, K, becomes proportional to $A^{2/3}$, where A is the mass number of the nucleus. The surface area of a sphere is proportional to its volume to the 2/3 power explaining the mass dependence. Due to this dependence, the frequency of the giant dipole resonance in the Goldhaber and Teller model is given by

$$\omega = \sqrt{\frac{K}{M}} \propto \sqrt{\frac{A^{2/3}}{A}} = A^{-1/6}. \tag{1.31}$$

This dependence describes light nuclei well, but it does not describe heavier nuclei [**?**]. The Steinwedel and Jensen model can be used to describe heavier nuclei. In this model, the proton and neutron fluids are confined to a single sphere where they are allowed to slosh back and forth creating the same effect as the Goldhaber and Teller model. Here there is no global separation of the proton and neutron fluids. The dipole is created by under-densities and over-densities of the proton and neutron fluids. It can be shown that this results in a frequency of oscillation which depends on one over the radius of the nucleus [**?**]:

$$\omega \propto \frac{1}{R} \propto A^{-1/3}. \tag{1.32}$$

As before, the relationship in Eq. 1.32 arises from the geometry of a sphere. The dependence of

the giant dipole resonance that is seen in the Steinwedel and Jensen model describes medium and heavier mass nuclei well. Empirically, both models are put together to give the following mass number dependence of the dipole resonance [**?**]

$$E_{GDR} = 32.2A^{-1/3} + 20.6A^{1/6}. \tag{1.33}$$

In order to compute the effect of an excitation in either model, the harmonic oscillator solutions found earlier can be driven by an interacting force. The resulting differential equation can then be solved using a Fourier transform to eliminate the time derivatives. In this model the driven harmonic has the following Lorentzian form:

$$\sigma_{GDR}(E_\gamma) = \frac{\sigma_{max} E_\gamma \Gamma_{GDR}^2}{\left(E_\gamma^2 - E_{GDR}^2\right)^2 + E_\gamma^2 \Gamma^2}, \tag{1.34}$$

where σ_{max} is the maximum cross section reached when $E_\gamma = E_{GDR}$; E_{GDR} is the peak resonance energy, and Γ_{GDR} is the width of the resonance. The width of this distribution lies in a range from 4-8 MeV and depends on the orbital arrangement to the neutrons and protons in the given nucleus [**?**].

For higher energy photons, the quasi-deuterium cross section is needed. The nucleus is treated as a collection of proton-neutron pairs, which are screened by the rest of the nucleus, in the quasi-deuterium approach. This behavior is modeled by [**?**]

$$\sigma_{QD}(E_\gamma) = L\frac{(L-A)Z}{A}\sigma_d(E_\gamma)F(E_\gamma), \tag{1.35}$$

where σ_d is the deuterium disintegration cross section for $\gamma + d \rightarrow p + n$; F is a function from Pauli blocking of fermions, and L is an empirical parameter set by data to 6.5 [**?**]. Certain energy levels are not available to the products of the deuterium disintegration process because of the presence of the rest of the nucleus. The result is a reduction of the cross section relative to free deuterium.

F can be modeled with an exponential cutoff below 20 MeV, a polynomial in the intermediate

range with nearly linear dependence on E_γ, and an inverted exponential above 140 MeV, pushing F to one at higher values of E_γ [**?**]. Essentially, the model at low photon energies disallows deuterium disintegration because the products have no available state to occupy, and at high energies the rest of the nucleus becomes transparent and looks more and more like a collection of deuterium. The deuterium disintegration cross section is found empirically and is fit to the following function [**?**]:

$$\sigma_d(E_\gamma) = 61.2\left(E_\gamma - 2.224\right)^{3/2}/E_\gamma. \tag{1.36}$$

In order to produce a final state for the target nucleus, a branching ratio is needed. The branching ratio gives the probability that the photo-excited nucleus will end up in a particular state. This determines the sort of emission that will result from the de-excitation process [**?**].

All the tools are now assembled to calculate the cross section for neutron emission. The first step in the calculation is to assume that the number of photons absorbed by either nucleus in the collision obeys the Poisson distribution [**?**, **?**]. The average number of absorptions as a function of impact parameter, $m(b)$,

$$m(b) = \int_{\omega_{min}}^{\omega_{max}} N(\omega, b)\sigma_{PN}(\omega)d\omega. \tag{1.37}$$

where σ_{PN} is the photo-nuclear cross section, and N is the photon flux (see Eq. 1.13).

In [**?**], the probability of any final state i due to the absorption of a single photon is given by

$$P_i(b) = \int_{\omega_{min}}^{\omega_{max}} P_a(b,1)q(b,\omega)f_i(\omega)d\omega = e^{-m(b)}\int_{\omega_{min}}^{\omega_{max}} N(b,\omega)\sigma_{PN}(\omega)f_i(\omega)d\omega, \tag{1.38}$$

where P_a is the probability that the target absorbs a single photon as calculated by following the Poisson distribution; q is the probability that the photon will have the frequency ω, and f_i is the branching ratio to a given final state. The following equation describes q [**?**]

$$q(b,\omega) = \frac{N(b,\omega)\sigma_{PN}(\omega)}{m(b)} \tag{1.39}$$

Integrating over the impact parameter to get an area that is weighted by the probability func-

tions gives [**?**, **?**]

$$\sigma_i = 2\pi \int_{b_0}^{\infty} bP_i(b)db. \tag{1.40}$$

Three parameters arise when calculating the cross section in Eq. 1.40, the minimum impact parameter b_0, the minimum emitted photon frequency ω_{min}, and the maximum emitted photon frequency ω_{max}. A minimum impact parameter ensures that the Bessel function in the photon flux in Eq. 1.13 is not evaluated at zero. At zero, the modified Bessel function does not converge. Physically, a minimum impact parameter is selected in order to separate the domains between electromagnetic interactions and the strong interactions that happen inside the nucleus. To serve this end, the minimum impact parameter is set to the radius of the nuclei [**?**, **?**]. This excludes collisions where the nuclei overlap in the calculation, and ensures that only electromagnetic interactions are involved.

1.6 Experimental Results

One of the first ~~UPC~~ results from RHIC was a UPC measurement, the measurement of the neutron spectrum from photon-induced nuclear break-up [**?**]. Neutrons due to the nuclear photon absorption are emitted with momenta on the order of the giant dipole resonance, about 60 MeV. Momenta of 60 MeV compared to the 100 GeV beam energy at RHIC result in neutron emission at very small angles, $\sim$ 2mrad, relative to the beam. These neutrons are captured by calorimeters, which are set in line with the beam called Zero Degree Calorimeters (ZDCs). These detectors are described in Section **??**. Figure 1.2 shows the charge recorded by the ZDCs. The peak at $\sim$ 30 in Fig. 1.2 is due to emission of a single neutron. Each successive peak is due to emission of an additional neutron. From these peaks, the cross section for nuclear break-up by neutron emission by both nuclei was measured. The fraction of nuclear interaction in all events with neutrons on both sides of the interaction point was found to be 0.661 ± 0.014 [**?**], which is in agreement the value 0.659 predicted by the model described in [**?**].

Nuclear collisions were separated from photon-induced break up by counting hits in the central scintillating counter similar to a tracker. Events with hits on both sides of the interaction point were

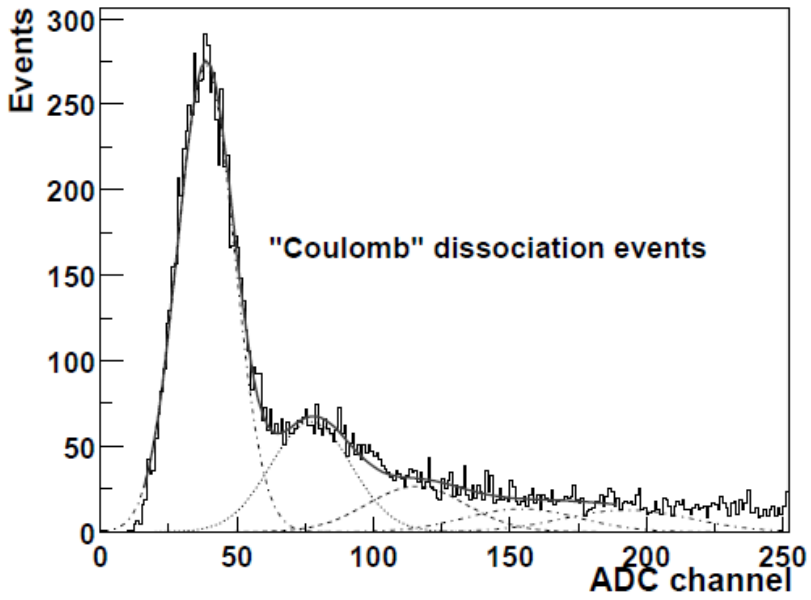

Figure 1.2: ZDC neutron spectrum at RHIC with each a Gaussian fit to the 1, 2, 3, 5, and 5 neutron peak [**?**].

categorized as nuclear interactions, and those with no hits or hits on only one side were categorized as electromagnetic interactions. The difference in the charge measured on each of the two sides of the interaction point, by the two ZDCs, is divided by the total charge for both ZDCs (see Fig. 1.3). Figure 1.3 shows that events created by electromagnetic interactions result in asymmetric neutron

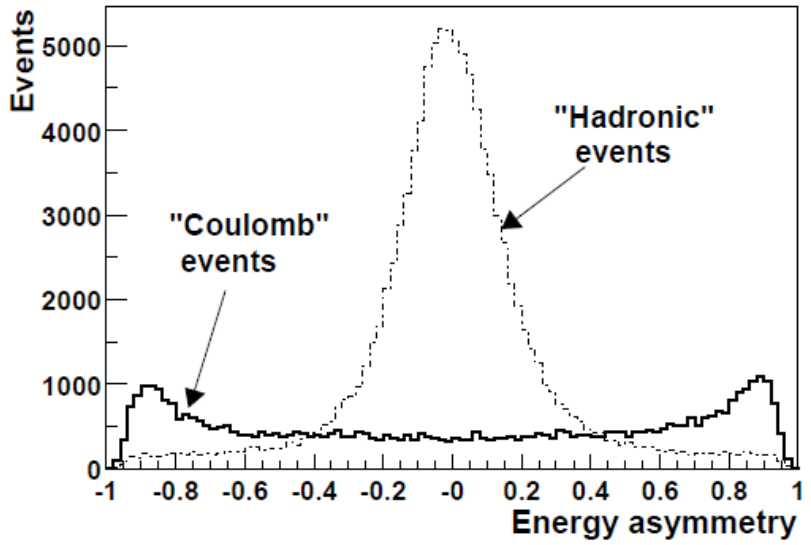

Figure 1.3: The energy asymmetry in the ZDCs for photon-induced interaction, coulomb events, and nuclear interaction, hadronic events [**?**].

emission, whereas nuclear interactions produce neutrons on both sides. In the analysis presented in this thesis, the energy asymmetry in the ZDCs is used to select UPC events. This will be discussed in Chapter **??**.

1.6.1 UPC vector mesons photoproduction at RHIC

Both the ρ^0 and J/ψ meson photoproduction cross sections in UPC events were measured at RHIC. STAR measured the photoproduction of the ρ^0 meson at collisions energies per nucleon of 62.4 GeV [**?**], 130 GeV [**?**], and 200 GeV [**?**]. The J/ψ was measured by PHENIX at 200 GeV [**?**]. The ρ measurements by STAR were in good agreement with the theory calculation method described in Section 1.2. The J/ψ measurement where limited by statistic as only 10 J/ψ candidates were found.

1.6.2 UPC J/ψ at the LHC

The increase in beam energy from 200 GeV at RHIC to 2.76 TeV at the LHC results in an increase in the Lorentz γ of about 10. Because the photon flux depends on γ^2, the photon flux at the LHC increases by a factor of about 100 compared to RHIC. All major heavy ion experiments, ALICE and CMS, have studied the production of UPC events. ALICE has studied coherent J/ψ photoproduction in ultra-peripheral PbPb collisions at $\sqrt{s_{NN}}$ = 2.76 TeV. The cross section for this process was measured at both forward-rapidity, y = 3, and mid-rapidity, y = 0. With an integrated luminosity of 55 μb^{-1}, ALICE measured 78 $\pm$ 10(stat) $^{+7}_{-11}$(syst) coherent J/ψ candidates at forward rapidity. The measured cross section was 1.00 $\pm$ 0.18(stat) $^{+0.24}_{-0.26}$ (syst) mb. For a symmetric system like PbPb collisions, as opposed to pPb collisions, there is an ambiguity between which ion is the target and which is the photon emitter. Therefore, the cross section has a contribution from the low-x and high-x parts of the gluon density. At y = 3 for PbPb collisions at the LHC, the cross section has a contribution from both $x = 5 \times 10^{-5}$ and $x = 2 \times 10^{-2}$. This ambiguity is not present at y = 0. ALICE has also measured the coherent J/ψ photoproduction cross section at y = 0, using a integrated luminosity of about 23 μb^{-1}. 291 $\pm$ 18 (stat)$\pm$ 4(syst) and 265 $\pm$ 40 (stat)$\pm$ 12(syst)

coherent J/ψ candidates were measured in the dimuon and dielectron channels, respectively. The combined cross section from both channels was measured to be 2.38 $^{+0.34}_{-0.24}$ (stat+syst) mb. At y = 0 $x \sim 10^{-3}$, which is a smaller x than at forward rapidity, and more sensitive to the nuclear gluon shadowing (see Fig. 1.4).

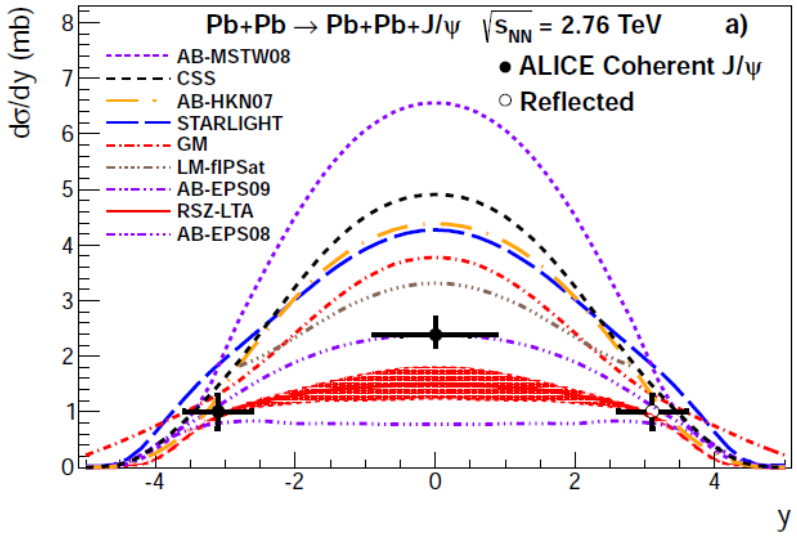

Figure 1.4: Coherent J/ψ photoproduction cross section in ultra-peripheral PbPb collisions at $\sqrt{s_{NN}}$ = 2.76 TeV, measured by the ALICE experiment at forward and mid-rapidity [].

The ALICE data points have been compared to several theoretical models. The UPC photoproduction cross section calculations depend significantly on how the nucleus is represented in the calculation. The results from the STARlight, LTA, and AB methods vary from a relatively large cross section in the STARlight model, ranging through a variety of values in the AB method, to a relatively small cross section in the LTA method. Each of these methods utilizes the same probe of the nucleus, the equivalent photon flux that is calculated using the Weizsäcker-Williams approximation (see Section 1.1). The three methods deviate in how they calculate the forward photoproduction scattering cross section. The differences in the UPC photoproduction cross sections predicted by the different models demonstrates the amount of experimental sensitivity there is to distinguishing between the models. The dependence of the cross section on rapidity is clearly visible.

The cross section value calculated by Eq. 1.22 in the STARlight, LTA, and the various gluon

Model	$\sigma_{AA\to AAJ/\psi}(mb)$
STARlight/STARlight MC	23
LTA	9
AB-MSTW08	34
AB-EPS08	7
AB-EPS09	14
AB-HKN07	23

Table 1.1: $\sigma_{AA\to AAJ/\psi}(mb)$ the LTA, STARlight, AB methods. Four different gluon density models are used in the AB method. STARlight is a simulation software package that utilizes the STARlight model.

density models in AB method vary significantly. Table 1.1 gives the predicted values for the three main methods taken from [**?**], [**?**], and [**?**]. The cross sections in Table 1.1 differ by a factor of 4 from the smallest to largest and create an experimental opportunity. The clear discrepancy between the models in Table 1.1 demonstrates the high amount of experimental sensitivity there is for distinguishing between the models.

The nuclear suppression factor, S, demonstrates the difference between how the models represent the nucleus. S is the ratio between the nuclear photoproduction cross section and the free nucleon photoproduction cross seciton. It is a measure of how the nuclear gluon densities evolve in each of the models. Figure. 1.5 from [**?**] shows the nuclear suppression, which is equivalent to R_g in Eq. 1.27, for the LTA and AB ~~method~~methods. Fig. 1.6 shows the nuclear suppression for the STARlight method [**?**]. Fig. 1.5 and Fig. 1.6 show that as the momentum of the probing photon goes up, increasing $W_{\gamma p}$, and momentum of the probed gluon goes down, decreasing x, the nuclear gluon density decreases relative to the free nucleon. The nuclear suppression factor, S, allows for the different models' representations of the gluon content of the nucleus to be directly compared to each other and to data. S can be measured from data by assuming a Weizsäcker-Williams photon flux and provides insight into nuclear gluon densities.

In addition, ALICE reported the measurement of the incoherent J/ψ photoproduction cross section at mid-rapidity. This provided additional constraints to the models for gluon shadowing.

In Chapter **??**, the coherent UPC J/ψ photoproduction cross section using CMS is described.

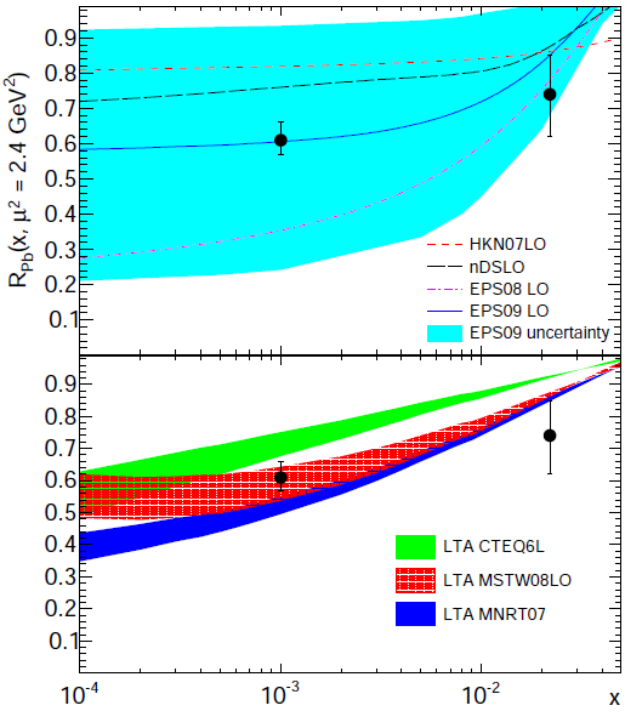

Figure 1.5: Nuclear supression factor, *S*, in the AB and LTA methods.

The measurement in this thesis adds to existing ALICE results, covering an intermediate range of x values.

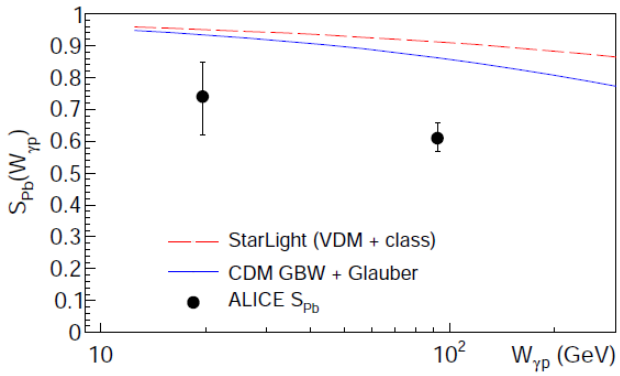

Figure 1.6: Nuclear supression factor, *S*, in STARlight method.